

Supplemental data for “Shock tunnel operation and correlation of boundary layer transition on a cone in hypervelocity flow”

J.S. Jewell¹, J.E. Shepherd¹, and I.A. Leyva²

1 Introduction

This is a supplemental report for “Shock tunnel operation and correlation of boundary layer transition on a cone in hypervelocity flow” by J.S. Jewell, J.E. Shepherd and I.A. Leyva [9], which is Paper 000300 in the 29th International Symposium on Shock Waves, held in Madison, WI, July 2013. It includes complete data sets and information on the statistical techniques used in data analysis, which were abbreviated in the main body of the paper.

2 Experiments

Experimental data are obtained in Caltech’s T5 Hypervelocity Reflected Shock Tunnel (see Hornung[7]). Flow conditions in T5 are calculated from three tunnel measurements: the shock speed, initial shock tube fill pressure and composition, and reservoir pressure at the end of the shock tube during the run time. Only experiments with measured shock speeds that fall within the uncertainty for the adjusted shock speed curve predicted by the shock jump conditions from the primary diaphragm burst pressure, driver gas composition, and initial shock tube conditions are included in the present data set.

Shock speed is measured by two time of arrival pressure transducers positioned 2.402 m apart, with an approximate measurement uncertainty of 8×10^{-6} s. The uncertainty in the shock speed measurement thus increases as the measured time of arrival difference decreases. At a shock speed of 3000 m/s, typical for the present study, the uncertainty is ~ 30 m/s. The shock tube fill pressure uncertainty is ~ 0.25 kPa, and the measured reservoir pressure uncertainty is typically ~ 4 MPa. Uncer-

California Institute of Technology, 1200 E. California Blvd., Pasadena, CA 91125, USA · Air Force Research Laboratory, 10 East Saturn Blvd., Edwards AFB, CA 93524, USA

tainties on the calculated quantities, including those represented by the error bars in Jewell et al.[9], are estimated by perturbing Cantera[6] condition computations[3] within the range of the uncertainties on the measured shock speed, reservoir pressure, and initial shock tube pressure. Only experiments with measured shock speeds that fall within the uncertainty for the adjusted shock speed curve predicted by the shock jump conditions from the primary diaphragm burst pressure, driver gas composition, and initial shock tube conditions are included in the present data set.

There are a number of other potential sources of measurement error, including nonideal gas behavior in the reservoir due to the high pressure, the extrapolation of the shock speed (which decays as it propagates down the shock tube) to the end wall, nonuniformity of reservoir conditions due to nonideal shock reflection, and the method of correcting flow conditions from the ideal reflected-shock pressure to measured reservoir pressure using an isentropic expansion. Furthermore, the 1-D contoured nozzle computation does not account for boundary layer growth within the nozzle, off-design operation conditions that lead to flow nonuniformity, or vibration-translation nonequilibrium and freezing within the nozzle, which is significant for the N_2 cases.

The experimental model is a 1 m smooth 5 degree half-angle cone, with a nominally sharp tip of radius 0.18 mm, instrumented with 80 thermocouples, providing heat transfer measurements from which transition location may be determined. Heat transfer results are normalized by Stanton number and Reynolds number, and the location of transition onset determined as described in Jewell et al.[8]

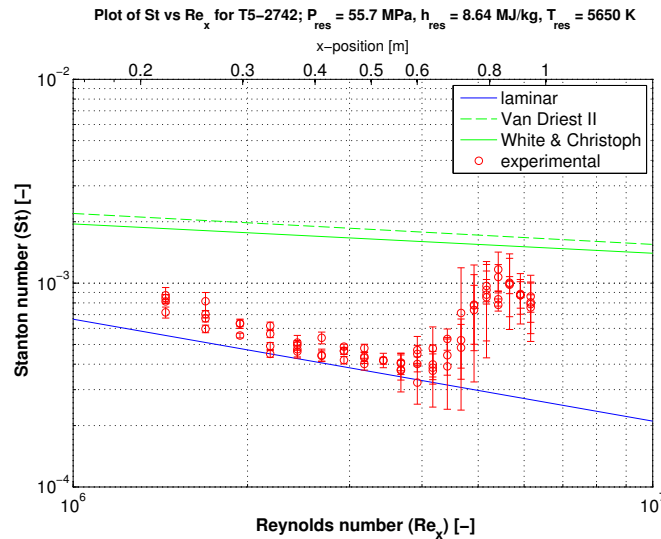


Fig. 1 Time-averaged non-dimensional plot of heat transfer results in terms of Stanton number vs. Reynolds number for T5 shot 2742 in air, with the laminar similarity correlation indicated in blue and two common turbulent correlations in green.

Heat transfer results for one experiment, in air at 8.64 MJ/kg and 55.7 MPa, are presented normalized by Stanton number and Reynolds number in Figure 1. Due to the distribution of the sensors around the circumference of the cone, in this representation of the data there are four results at each of 20 x -locations. The circles represent the time-averaged heat transfer result over the ~ 1 ms steady flow time, and the bars represent the root mean squared values from each sensor over the steady flow time. The RMS bars are initially small in the laminar zone as the heat transfer values are consistently at the laminar value, increase in size in the transitional zone as the flow becomes intermittent, and may then decrease in size again as the flow approaches the fully turbulent zone and heat transfer levels are consistently near the turbulent value. A slight drop-off from the maximum heat transfer value is observed in the last rows of thermocouples, as they are positioned near the maximum extent of the T5 test rhombus and may intersect with the expansion fan emanating from the lip of the nozzle. For this experiment, transition onset is observed at 0.59 m from the tip of the cone, and the transitional zone extends at least 0.20 m beyond the observed onset location before fully turbulent flow is achieved.

Datasets of experiments in which transition onset is clearly observed are presented for all N_2 conditions ($n = 10$) in Table 1, and all air conditions ($n = 24$) in Table 2. The calculated boundary layer thickness $\delta_{.99}$ and the approximate most amplified Mack second mode[11] frequency $f \approx 0.6U_e/2\delta_{.99}$ at the observed transition location are also reported.

3 Previous Results

Datasets in air ($n = 22$) from shots referenced by Adam[1] and Adam and Hornung[2] are presented in Table 3. Some of these experiments were performed by, and first referenced in, Germain and Hornung[5]. Observed transition onset location X is reproduced here as reported in [1], but the other parameters have been recalculated by the present methods for consistency. In the case of Re^*/m for Dorrance reference conditions, $\delta_{.99tr}$, and f_{tr} , the parameters have been calculated here for the first time.

Table 1 Experiments performed in N_2 , with unit Reynolds numbers evaluated at the boundary layer edge and Dorrance reference conditions, observed transition onset location, and δ and f calculated at the transition onset location.

	h_{res} [MJ/kg]	P_{res} [MPa]	Re/m [1/m]	Re^*/m [1/m]	X_{tr} [m]	δ_{99tr} [mm]	f_{tr} [kHz]
2772	8.00	16.7	2.31×10^6	1.35×10^6	0.67	2.18	515
2773	8.99	16.7	2.02×10^6	1.25×10^6	0.67	2.26	522
2775	7.26	17.4	2.67×10^6	1.49×10^6	0.67	2.07	519
2776	7.17	45.9	7.09×10^6	3.94×10^6	0.39	0.97	1102
2777	8.91	38.9	4.67×10^6	2.89×10^6	0.49	1.28	924
2778	10.73	41.4	3.99×10^6	2.72×10^6	0.55	1.41	910
2779	12.00	42.3	3.57×10^6	2.56×10^6	0.60	1.53	881
2780	13.64	44.5	3.23×10^6	2.46×10^6	0.62	1.59	891
2782	14.84	53.9	3.47×10^6	2.76×10^6	0.61	1.50	980
2783	15.88	53.3	3.20×10^6	2.62×10^6	0.63	1.56	966

Table 2 Experiments performed in air, with unit Reynolds numbers evaluated at the boundary layer edge and Dorrance reference conditions, observed transition onset location, and δ and f calculated at the transition onset location.

	h_{res} [MJ/kg]	P_{res} [MPa]	Re/m [1/m]	Re^*/m [1/m]	X_{tr} [m]	δ_{99tr} [mm]	f_{tr} [kHz]
2714	9.49	67.1	6.85×10^6	5.03×10^6	0.49	1.00	1183
2715	10.48	68.8	6.24×10^6	4.79×10^6	0.70	1.22	1004
2716	10.79	67.4	5.90×10^6	4.57×10^6	0.72	1.27	981
2739	8.03	57.5	7.28×10^6	4.90×10^6	0.55	1.06	1033
2740	7.97	57.3	7.32×10^6	4.91×10^6	0.54	1.04	1049
2741	8.34	56.9	6.85×10^6	4.70×10^6	0.57	1.09	1023
2742	8.64	55.7	6.54×10^6	4.58×10^6	0.58	1.14	997
2743	9.09	56.3	6.17×10^6	4.43×10^6	0.64	1.25	926
2744	7.68	60.7	8.19×10^6	5.39×10^6	0.51	0.98	1094
2753	8.66	52.1	6.05×10^6	4.22×10^6	0.68	1.27	891
2758	11.07	72.0	6.11×10^6	4.79×10^6	0.74	1.26	1002
2759	9.62	60.4	6.12×10^6	4.51×10^6	0.68	1.23	959
2760	6.29	27.2	4.76×10^6	2.72×10^6	0.51	1.34	730
2761	5.49	28.2	5.80×10^6	3.04×10^6	0.49	1.24	744
2762	6.06	27.8	5.11×10^6	2.86×10^6	0.51	1.31	736
2763	6.56	27.2	4.52×10^6	2.66×10^6	0.53	1.40	716
2764	5.27	16.5	3.62×10^6	1.83×10^6	0.52	1.65	551
2765	6.47	17.5	3.03×10^6	1.74×10^6	0.65	1.90	522
2766	7.54	17.0	2.49×10^6	1.55×10^6	0.64	2.01	526
2769	10.46	60.8	5.61×10^6	4.28×10^6	0.64	1.23	999
2786	10.03	53.6	5.22×10^6	3.90×10^6	0.65	1.30	929
2787	10.72	54.7	4.93×10^6	3.76×10^6	0.61	1.28	971
2789	11.87	56.4	4.52×10^6	3.55×10^6	0.73	1.44	897
2790	11.55	57.4	4.77×10^6	3.74×10^6	0.68	1.36	944

Table 3 Experiments performed in air referenced in Adam[1] and Adam and Hornung[2], with unit Reynolds numbers evaluated at the boundary layer edge and Dorrance reference conditions, observed transition onset location, and δ and f calculated at the transition onset location. Observed transition onset location X is as reported in [1], but the other parameters have been recalculated by the present methods for consistency, and in the case of Re^*/m , δ , and f , calculated here for the first time.

	h_{res} [MJ/kg]	P_{res} [MPa]	Re/m [1/m]	Re^*/m [1/m]	X_{tr} [m]	δ_{99tr} [mm]	f_{tr} [kHz]
675	10.20	58.5	5.60×10^6	4.23×10^6	0.54	1.13	1074
683	10.43	65.5	5.94×10^6	4.51×10^6	0.41	0.96	1280
684	11.10	60.9	5.25×10^6	4.09×10^6	0.46	1.07	1180
685	10.32	56.9	5.37×10^6	4.06×10^6	0.43	1.04	1178
686	12.95	55.4	4.02×10^6	3.20×10^6	0.59	1.38	974
687	13.06	57.3	4.14×10^6	3.33×10^6	0.59	1.35	1001
688	13.27	62.3	4.38×10^6	3.55×10^6	0.62	1.33	1018
689	10.65	59.0	5.34×10^6	4.09×10^6	0.54	1.15	1070
879	11.65	79.1	6.26×10^6	5.00×10^6	0.49	1.00	1289
888	11.55	79.1	6.28×10^6	4.97×10^6	0.63	1.14	1124
1113	11.37	77.2	6.34×10^6	5.04×10^6	0.48	0.98	1293
1115	7.38	68.7	9.66×10^6	6.20×10^6	0.43	0.83	1275
1151	10.03	45.0	4.46×10^6	3.29×10^6	0.57	1.32	907
1152	8.88	43.3	4.97×10^6	3.50×10^6	0.40	1.06	1076
1153	12.19	40.7	3.30×10^6	2.53×10^6	0.72	1.70	769
1155	8.08	44.3	5.66×10^6	3.80×10^6	0.45	1.09	1007
1156	7.80	48.0	6.34×10^6	4.18×10^6	0.39	0.96	1124
1157	5.83	47.2	8.94×10^6	4.90×10^6	0.23	0.67	1421
1159	11.41	42.5	3.67×10^6	2.80×10^6	0.72	1.61	788
1160	10.41	41.9	4.00×10^6	2.98×10^6	0.66	1.49	819
1162	9.04	34.4	3.91×10^6	2.74×10^6	0.60	1.48	773
1163	11.17	68.1	5.73×10^6	4.47×10^6	0.59	1.15	1094

4 Statistical Analysis

Multivariable linear regression analysis is performed on these data sets with the MATLAB Statistics Toolbox, taking P_{res} and h_{res} (normalized by each data set's maximum pressure and enthalpy) as the possible predictor variables and the measured values of X_{tr} (normalized by the length of the cone, 1 m), Re_{tr}^* and Re_{tr} (normalized by the respective maximum unit Reynolds numbers) as the modeled variables. We use a significance level of 5% (i.e. requiring a p -value less than 0.05 to reject the null hypothesis that a given coefficient is zero). The linear model coefficients that result from this analysis, along with their respective p -values, are presented in Tables 4, 5 and 6. Note that these tables include the results of statistical analysis for Re_{tr} in addition to X_{tr} and Re_{tr}^* , although only the latter two parameters are referenced in the main paper[9].

Both the present N_2 and air results have a positive dependence on h_{res} (linear model coefficient 0.56 for N_2 , 0.55 for air) and a negative dependence on P_{res} (-0.45 for N_2 , -0.15 for air; note that the air result, with p -value = 0.054, is marginal). The historical air data of Adam and Hornung[2] are analyzed in the same way, and likewise show a significant positive dependence of X_{tr} on h_{res} (0.72) and negative dependence on P_{res} (-0.28).

Both the present N_2 and air results have a positive dependence on P_{res} (linear model coefficient 0.31 for N_2 , 0.59 for air) for the transition Reynolds number evaluated at Dorrance reference conditions, Re_{tr}^* , but neither have a dependence on h_{res} that is statistically significant. The historical air data of Adam and Hornung[2] likewise show a significant positive dependence of Re_{tr}^* on P_{res} (0.34), but no statistically significant dependence on h_{res} .

No statistically significant correlation of Re_{tr}^* with reservoir enthalpy h_{res} is observed for any data set, either in the present data or in a statistical re-examination of Adam and Hornung[2], who reported an increase in Re_{tr}^* with increasing h_{res} , but did not control for P_{res} , which varied from 10 to 85 MPa in their air experiments. In both present and past data, Re_{tr}^* appears to correlate most strongly with P_{res} .

Table 4 Multivariable linear regression analysis for N_2 results ($n = 10$) from the present study. P_{res} and h_{res} are normalized by their respective maximum values. The coefficients found to be statistically significant ($p < 0.05$) are in bold print.

	X_{tr}	Re_{tr}^*	Re_{tr}
P_{res} coefficient	-0.45396	0.30819	0.29023
p -value	1.20×10^{-5}	5.88×10^{-6}	7.89×10^{-7}
h_{res} coefficient	0.55527	-0.02805	-0.26922
p -value	2.36×10^{-5}	0.44139	1.02×10^{-5}

Table 5 Multivariable linear regression analysis for air results ($n = 24$) from the present study. P_{res} and h_{res} are normalized by their respective maximum values. The coefficients found to be statistically significant ($p < 0.05$) are in bold print. Note that the P_{res} coefficient for X_{tr} in this data, which has $p = 0.054$, is of marginal significance.

	X_{tr}	Re_{tr}^*	Re_{tr}
P_{res} coefficient	-0.15238	0.58556	0.54107
p -value	0.05377	1.72×10^{-9}	7.30×10^{-10}
h_{res} coefficient	0.54802	-0.04254	-0.28748
p -value	7.39×10^{-5}	0.62997	0.00117

Table 6 Multivariable linear regression analysis for historical air results ($n = 22$) referenced in Adam[1]. P_{res} and h_{res} are normalized by their respective maximum values. The coefficients found to be statistically significant ($p < 0.05$) are in bold print.

	X_{tr}	Re_{tr}^*	Re_{tr}
P_{res} coefficient	-0.28405	0.33725	0.27436
p -value	0.01308	3.07×10^{-4}	3.24×10^{-4}
h_{res} coefficient	0.72414	0.10048	-0.043046
p -value	1.23×10^{-5}	0.28530	0.57148

References

1. Adam P.H. (1997) Enthalpy Effects on Hypervelocity Boundary Layers. PhD Thesis, California Institute of Technology, Pasadena, CA 91125.
2. Adam P.H. and Hornung H.G. (1997) Enthalpy Effects on Hypervelocity Boundary-Layer Transition: Ground Test and Flight Data. *Journal of Spacecraft and Rockets*, Vol. 34, No. 5, pp. 614–619.
3. Browne S., Ziegler J. and Shepherd J.E. (2008) Numerical solution methods for shock and detonation jump conditions. GALCIT Report FM2006.006.
4. Dorrance W.H. (1962) *Viscous Hypersonic Flow: Theory of Reacting and Hypersonic Boundary Layers*. McGraw-Hill.
5. Germain P. and Hornung H.G. (1997) Transition on a Slender Cone in Hypervelocity Flow. *Experiments in Fluids*, Vol. 22, pp. 183–190.
6. Goodwin D. (2009) Cantera: An object-oriented software toolkit for chemical kinetics, thermodynamics, and transport processes. California Institute of Technology. Available: <http://code.google.com/p/cantera>.
7. Hornung H.G. (1992) Performance data of the new free-piston shock tunnel at GALCIT. AIAA 92-3943.
8. Jewell J.S., Wagnild R.M., Leyva I.A., Candler G.V. and Shepherd J.E. (2013) Transition within a hypervelocity boundary layer on a 5-degree half-angle cone in air/CO₂ mixtures. AIAA 2013-0523.
9. Jewell J.S., Shepherd J.E., and Leyva I.A. (2013) Shock tunnel operation and correlation of boundary layer transition. *Proceedings of the 29th International Symposium on Shock Waves*, Madison, WI. Paper ISSW29-000300.
10. Leyva I.A., Jewell J.S., Laurence S., Hornung H.G. and Shepherd J.E. (2009) On the impact of injection schemes on transition in hypersonic boundary layers. AIAA 2009-7204.
11. Mack L.M. (1984) Boundary-layer stability theory. *Special Course on Stability and Transition of Laminar Flow*. AGARD Report 709.